Accepted Manuscript

Electrochemical approach for monitoring the effect of anti tubulin drugs on breast cancer cells based on silicon nanograss electrodes

Somayeh Zanganeh, Safoora Khosravi, Naser Namdar, Morteza Hassanpour Amiri, Milad Gharooni, Mohammad Abdolahad

PII: S0003-2670(16)30878-9

DOI: 10.1016/j.aca.2016.07.042

Reference: ACA 234724

To appear in: *Analytica Chimica Acta*

Received Date: 19 May 2016

Revised Date: 29 July 2016

Accepted Date: 31 July 2016

Please cite this article as: S. Zanganeh, S. Khosravi, N. Namdar, M.H. Amiri, M. Gharooni, M. Abdolahad, Electrochemical approach for monitoring the effect of anti tubulin drugs on breast cancer cells based on silicon nanograss electrodes, *Analytica Chimica Acta* (2016), doi: 10.1016/j.aca.2016.07.042.

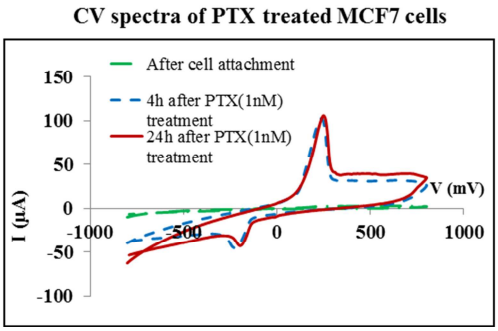

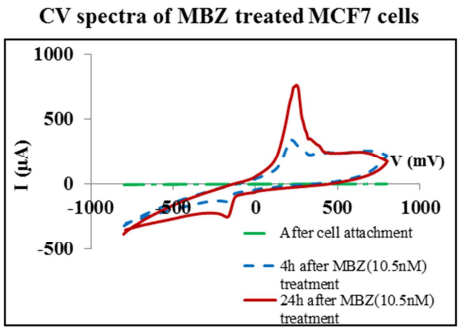

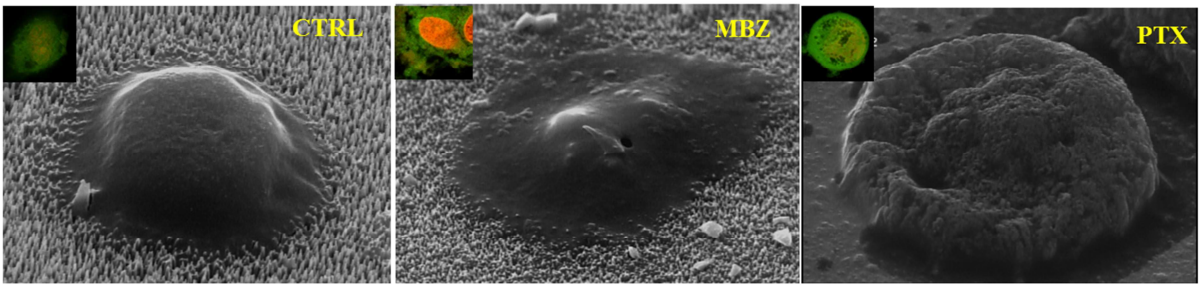

Electrochemical approach for monitoring the effect of anti tubulin drugs on breast cancer cells based on silicon nanograss electrodes

Somayeh Zanganeh [a,b,#], Safoora Khosravi [a,b], Naser Namdar [a,b,†], Morteza Hassanpour Amiri [a,b,†], Milad Gharooni [a,b], Mohammad Abdolahad [a,b,#,*]

[a] Nano Electronic Center of Excellence, Nano Bio Electronic Devices Lab, School of Electrical and Computer Eng, University of Tehran, Tehran, Iran, P.O. Box 14395/515, Tehran, Iran

[b] Nano Electronic Center of Excellence, Thin Film and Nanoelectronic Lab, School of Electrical and Computer Eng, University of Tehran, Tehran, Iran, P.O. Box 14395/515, Tehran, Iran

***Corresponding Author: m.abdolahad@ut.ac.ir,**

[#,†] Authors with same collaboration

Abstract

One of the most interested molecular research in the field of cancer detection is the mechanism of drug effect on cancer cells. Translating molecular evidence into electrochemical profiles would open new opportunities in cancer research. In this manner, applying nanostructures with anomalous physical and chemical properties as well as biocompatibility would be a suitable choice for the cell based electrochemical sensing. Silicon based nanostructure are the most interested nanomaterials used in electrochemical biosensors because of their compatibility with electronic fabrication process and well engineering in size and electrical properties. Here we apply silicon nanograss (SiNG) probing electrodes produced by reactive ion etching (RIE) on silicon wafer to electrochemically diagnose the effect of anticancer

drugs on breast tumor cells. Paclitaxel (PTX) and mebendazole (MBZ) drugs have been used as polymerizing and depolymerizing agents of microtubules. PTX would perturb the anodic/cathodic responses of the cell-covered biosensor by binding phosphate groups to deformed proteins due to extracellular signal-regulated kinase ($ERK^{1/2}$) pathway. MBZ induces accumulation of Cytochrome C in cytoplasm. Reduction of the mentioned agents in cytosol would change the ionic state of the cells monitored by silicon nanograss working electrodes (SiNGWEs). By extending the contacts with cancer cells, SiNGWEs can detect minor signal transduction and bio recognition events, resulting in precise biosensing. Effects of MBZ and PTX drugs, (with the concentrations of 2nM and 0.1 nM, respectively) on electrochemical activity of MCF-7 cells are successfully recorded which are corroborated by confocal and flow cytometry assays.

Keyword: cancer cell, electrochemical response, silicon nanograss, mebendazole and paclitaxel drug, cyclic voltammetry, biosensor.

1. Introduction

Electrochemical biosensors are capable of transducing biochemical interactions to detectable electrical signals [1]. Biomarkers (e.g., enzymes, aptamers or antibodies), as the main part of the signal transmission, ought to be linked to the sensitive interface to mediate the sensing procedure [2, 3]. However, limitations in types of suitable linkers, non-specific binding and complex chemical modifications perturb the reliability and accuracy of such biosensors. One of the newest

challenges in electrochemical technology is replacing the marker based detection by label-free procedures. If the oxidative/reductive electrochemical responses of an analyte were unique in different biological transformations, we would achieve label-free sensing patterns.

Applying nanomaterials in interfacial modification of electrochemical biosensors greatly extended the range of response and enhanced the sensing performance depending on their sizes and shapes. Great physiochemical interactions with anomalous charge transfer ability were some of the characteristics reported for many nanostructures applied in electrochemical biosensing [4, 3, 5, 6].

Moreover, if the biocompatibility of nanostructures would be acceptable, sensing interfaces produced by nanostructures would present new generation of label free biosensors for monitoring vital cells.

Among various biocompatible nanomaterials with good electron transport properties, silicon based nanostructures, such as silicon nanowire (SiNW), silicon nanotube (SiNT) and silicon nanograss (SiNG) were noticeably considered in biosensing approaches because of their greatly controllable conductivity [7, 8], enlarged electrochemically active area and well compatibility with silicon fabrication processes [9]. Many electrical biosensors were developed based on SiNW arrays such as SiNW bio field effect transistor (bio FET) and SiNW based electrical cell impedance sensor (SiNW-ECIS) [10] for cancer cell detection as well as SiNW kinked transistor for signal extraction from cardiomyocyte cells [11]. Main disadvantage of SiNWs is using the gold catalyst in growth mechanism as a non-compatible material by FET fabrication process. Also engineering the size of SiNWs in low pressure chemical vapor deposition (LPCVD) or metal assisted etching systems wouldn't be simple. SiNGs are nanostructures which have been formed on silicon substrate with the assistance of reactive ion etching (RIE) as a simple and FET

compatible process by fine aspect ratio and great charge transport properties [12]. It also presented well biological interaction with cells [13]. In this paper, we attempt to apply SiNG based electrochemical probes in interaction with breast cancer cells to assay the effect of anticancer drugs on their function and metabolism. The sensing has been based on monitoring the anodic/cathodic responses of the cell-covered probes after drug incubation. Formation of nanograsses on the surface of silicon substrate, increases the interactive surface with electrodes. Mebendazole (MBZ) and paclitaxel (PTX) are selected as anti-tubulin drugs to make non-regulated depolymerization and polymerization on cancer cells, respectively [14]. Cyclic voltammetry (CV) and differential pulse voltammetry (DPV) responses of breast cancer cells (MCF-7 cell line) are measured after their interaction with various doses of the drugs and the data is compared with control samples. Confocal and flow cytometry assays are also investigated as reference biological data to evaluate the validity of electrochemical results. SiNG probes serves as a good candidate for new generation of drug resistance biosensors in the field of cancer.

2. Materials and methods

2.1. Biosensor fabrication process

Silicon substrates were cleaned through standard cleaning method named RCA#1 (NH_4OH:H_2O_2:H_2O solution and volume ratio of 1:1:5 respectively). The surface of the wafer was then processed by RIE system (SensIran Co.) to form nanograss structures.

The grass formation was carried on by a radio frequency (RF)-plasma (13.56 MHz) in the ambient of mixed oxygen, hydrogen and sulfur-hexafluoride (SF6) gases with consecutive steps of passivation and etching sub-cycles [12]. H_2 and O_2 gases were mixed with the flows of 100

and 80 standard cubic centimeter per minute (SCCM) during the passivation step, respectively. A minor trace of SF_6 was also applied in this step. The plasma power and duration of the passivation step were 150W and 50s, respectively. The etching step is conducted under the plasma power of 130W for 10s using about 30 SCCM of SF_6 as inlet gas. Incorporating such procedure, various features are obtained on silicon substrates with sizes down to 100nm in width. Finally, the nanograss substrate was located in phosphorous doping furnace to enhance the electrical conductivity of electrodes. The doping was conducted in the presence of Phosphorus oxychloride ($POCl_3$) in 850^{o}C.

2.2. Cell culture and drug incubation

MCF-7 cell lines obtained from the national cell bank of Iran (Pasteur Institute) had been isolated from grade I human breast tumors. Cells were maintained at CO_2 incubator (37 °C, 5% CO_2) in RPMI-1640 medium (Sigma) supplemented with 5% fetal bovine serum (Sigma) and 1% penicillin/streptomycin (Gibco). The fresh medium was replaced every other days. Prior to each experiment, cells were detached by trypsinization from the substrate and resuspended on the SiNG electrodes. To minimize the effect of trypsinization, the procedure was taken less than 4 minutes at room temperature around 20-22^{o}C. We held the samples in incubator for 4h to achieve cells attachment on the SiNGs. Then, the MBZ and PTX drugs with various concentrations were added to individual samples. Such doses were 2.1 and 10.5 nM for MBZ and 0.1 and 1 nM for PTX drugs. The signal recording and biological assays were investigated 2, 6 and 10 hours after addition of the drugs.

2.3. Electrochemical measurement procedure

Electrochemical CV test was performed using three electrode electrochemical cyclic voltammetry RNFPG Stat system (Roshd Nanofanavaran Co. Iran). SiNG electrode was utilized as working electrode (WE) in a fixed separation in the presence of standard reference electrode (RE) made by Ag/AgCl and counter electrode (CE) made by platinum. CV was performed between the SiNGWE and CE in the presence of RE biased at a fixed potential. Measurements were carried out at -0.8 to 0.8 V at a scan rate of 100mV/s.

For DPV measurement, the current was sampled before and during the pulse application. The current was measured immediately before each potential change and the current difference was plotted as a function of potential. It is important to note that we replaced media solution of drug treated cells by conventional RPMI to inhibit any non-desirable ionic signals of drug solution.

2.4. Confocal imaging

MCF-7 cells were grown on individual glass slides and treated with 2.1 and 10.5 nM MBZ for 2h. In addition, control (CTRL) sample, treated with no drugs, was prepared as reference for comparison. Samples were then washed with phosphate buffer solution (PBS) and permeabilized with microtubule (MT) stabilizing buffer [80 mM PIPES-KOH (pH 6.8), 5 mM EGTA, and 1 mM $MgCl_2$ containing 0.5% Triton X-100] for 5 min at room temperature before being fixed with chilled absolute methanol for 10 min at –20°C. Fixed cells were washed and incubated with monoclonal mouse anti-α-tubulin antibody (Sigma) for 1 h at room temperature followed by incubation with FITC-conjugated antimouse IgG antibody (Santa Cruz Biotechnology). The stained cells were mounted with Vectashield (Vector Laboratories, Burlingame, CA) and observed by confocal microscopy.

2.5. Cell cycle analysis by flow cytometry

For cell cycle investigation by flow cytometry, cells were harvested, washed in PBS, and fixed in 70% methanol. The fixed cells were then incubated with 0.65 µg/ml mouse monoclonal anti-MPM-2 antibody. Cells were then incubated with 2 µg/ml FITC-conjugated goat antimouse IgG secondary antibody (Santa Cruz Biotechnology, Santa Cruz, CA), 20 µg/ml PI (Roche Diagnostics), and 10 µg/ml RNase A (Sigma-Aldrich) at 37°C for 30 min. Then, the cell cycle analysis was performed using an EPICS Profile II flow cytometer (Coulter Corp., Miami, FL) with the Multicycle Phoenix Flow Systems program (San Diego, California).

3. Results

3.1. Structural characteristics of SiNG

Fig. 1 A1, A2, B2 and B3 present field emission scanning electron microscopy (FESEM), 2D and 3D atomic force microscopy (AFM) images of the nanograss surface. It is observable from FESEM (Fig. 1A1) and 3D AFM (Fig. 1A3) images that about 60 grass features are formed in 1 μm^2 of the surface. The height of the grasses is about 1 µm (Fig. 1A3) with the sharp cone of about 100nm (Fig. 1A1). Also FESEM image taken from cell-covered nanograsses (Fig. 1B1) indicates their 3D interfacial surface with the attached cell.

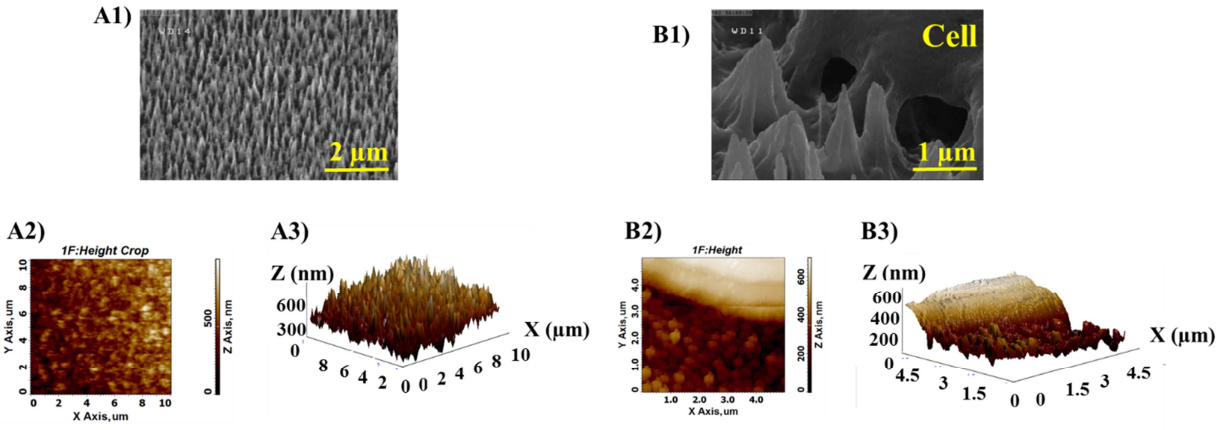

Fig. 1. A1) FESEM image of SiNG surface. The geometry and distribution of the grasses is observable in the figure. As indicated in 2D (A2) and 3D (A3) AFM images of the nanograsses, the average roughness of the Si substrate is increased after indentation of the grasses. B1) FESEM micrographs from the direct interfaces between cell membrane and nanograsses. Cell outer wall covers the conical surface of interacted grasses.

The interactive surface of $1\mu m^2$ in bare silicon electrode after indentation of SiNG structures was increased to about 200 μm^2. This increment initiated from the added outer surface of silicon conical grasses formed in the substrate. On the other hand, the interactive surface between a seeded cell and smooth silicon substrate was about πR^2_{cell} [15]. After producing nano features, this surface would be increased by similar cofactors. After interaction of the cells with SiNGs, well binding sites were applied between cells outer membrane and SiNG arrays with no tears or retraction (Fig. 1B1, B2 and B3).

Enhanced interactive surface between Si substrate with nanograss morphology and attached cells provide unique electrochemical characteristics due to their high surface area and excellent ability of the boundaries in sensing any electrochemically produced charges through the connected net of grass crystals.

3.2. Electrochemical characterization of SiNGWE

Electrochemical response of SiNGWEs was analyzed by cyclic voltammetry at scan rate of 100 mV/s in the presence of 0.01 M of Potassium Ferricyanide ($K_3Fe(CN)_6$) as a standard ionic solution to test the response of an electrochemical system. The obtained results are shown in **Error! Reference source not found.**2A1, A2. Presence of both anodic and cathodic current peaks of SiNGWEs located at -300 and 280 mV reflect their desired electrochemical signal extraction, respectively. The absolute peak current of DPV is about 160 µA.

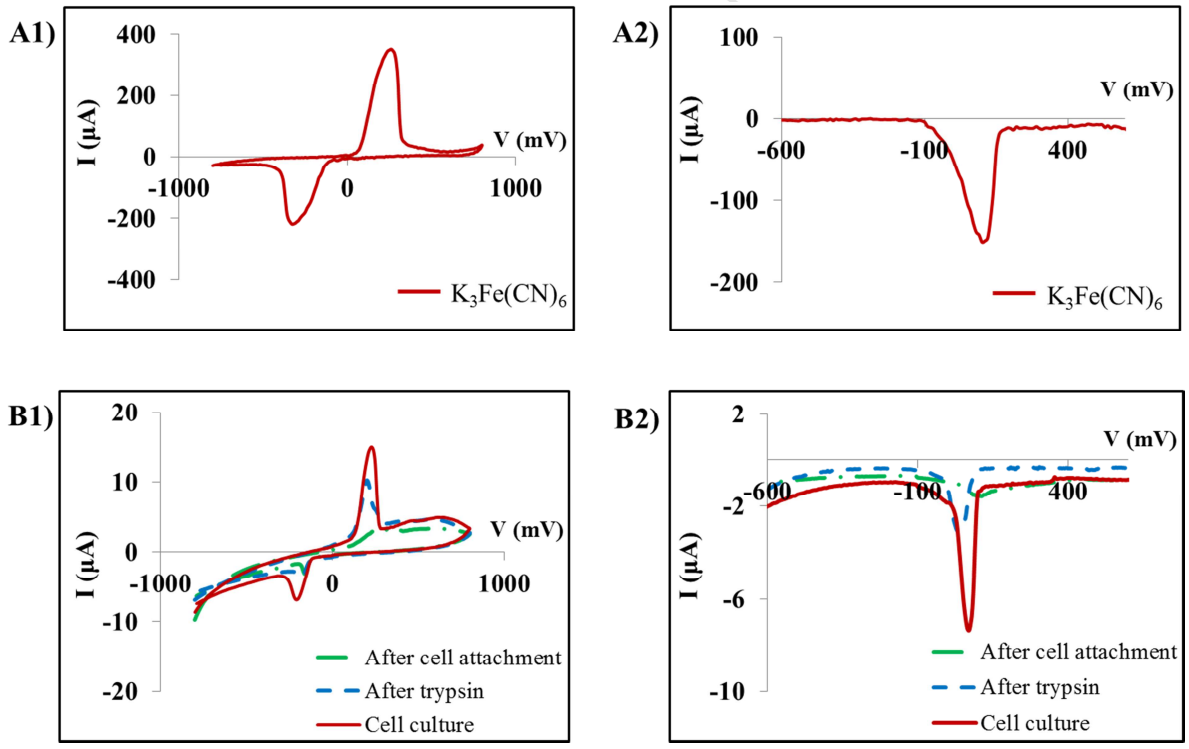

Fig. 2. A1) CV and A2) DPV of Potassium Ferricyanide ($K_3Fe(CN)_6$) as standard ionic solution measured by SiNG working electrode. Sharp anodic and cathodic spikes are observable in 260mV and -320mV.

Also, the DPV current is about -160µA. Panel B showes the CV (B1) and DPV (B2) diagrams of SiNGWEs in the presence of media solution (solid line), after cells attachment on the electrodes (dashed dotted line) and after detachment of the cells from the electrode by trypsin (dashed line). Presence of the cells strongly reduces the anodic/cathodic spikes of the SiNGWEs. An offset can also be observed between the response of the sensor before cell attachment and after cell trypsinization.

To investigate the application of SiNGWEs in assaying the drug resistance of cancer cells, we first measured the CV and DPV responses of the electrode in the presence of RPMI1640 ionic solution (contained 10% FBS) as the cell culture media. The cells would be maintained and grown in RPMI and its effect must be considered in evaluating the electrochemical responses of the cells either before or after drug treatment. The anodic peak of RPMI sensed by SiNGWEs was about -5 µA located at the voltage of about -200mV (Fig. 2B1 solid line). In addition, SiNGWEs presented a fine DPV peak of -5µA for RPMI (Cell culture). In next step, the MCF-7 cells were suspended in media solution and exposed to SiNGWE. We held the electrode in incubator for at least 4h to let the cells attach on nanograss surface. As shown in Fig. 2B, electrochemical spikes strongly decreased after attachment of MCF-7 cells on SiNGWEs (Anodic peak reduced to -0.8 µA located at -150mV). Dielectric nature of cells membrane covered on electrodes might act as an insulating layer, suppressing ionic current.

Fig. 2B2 (dotted dashed line) presents a reduced DPV current peak after attachment of cancer cells on nanograss electrodes (absolute DPV current reduced to 0.8µA). Such considerable reduction would be an indication of well electrochemical sensitivity of SiNGs to bio evidences.

To examine the repeatability of the SiNGWE, measurements were repeated after detachment of MCF-7 cells from the surface of nanograsses by trypsinization (as mentioned in experimental section). Fig. 2B1 (blue dashed line named After Trypsin) depicts the response of the SiNGWE covered by cell culture media after detachment of the cells from the surface. It can be seen that

anodic spike again is increased in negative regime (-2.5µA located at -170mV). Similarly, absolute value of DPV current is increased to 2.5µA (Fig. 2B2 dashed line). Removing the cells from the electrodes by trypsinization, results in an ionic current path from SiNGWE to CE. An offset in the electrochemical spikes of SiNGWEs between culture media and removed cells states, might be initiated from remained adhesive proteins of the cells after trypsinization which prevents the precise adjustment of the peak current in its previous location (solid vs. dashed lines in Fig. 2B2).

3.3. Electrochemical response of SiNGWEs to microtubule polymerizing/ depolymerizing drugs

Any ionic non-equilibrium induced by anticancer drugs could result in a change in ionic current and biochemical behavior of cancer cells. Such variations were tracked in electrochemical responses of SiNGWEs covered by cancer cells, before and after drug treatment. Here, we utilize antitubulin drugs (MBZ and PTX) as clinically applicable biochemical perturbing agents in mitosis of cancer cells.

Fig. 3A1, 2 and 3B1, 2 present the CV and DPV diagrams of CTRL and MBZ treated samples with individual concentrations of 2 and 10.5nM, respectively. Considerable appearance of anodic and cathodic spikes were noticeable in CV scan of the SiNGWEs just 4h after incubation of the drug with the attached cells (As evident from Fig. 2B1, cells covered electrode shows very minor electrochemical spikes). Fig. 3A1 (dashed line) indicates that treating the cells by 2nM of MBZ increases the anodic peak of the response to about 60µA. Similarly, the DPV current peak (absolute value) of the sensor increased from 1.5µA (Fig. 3A2 dotted dashed line) to 27 µA (Fig. 3A2 dashed line). 24h after the drug treatment, the anodic and DPV peaks reached to 80µA (Fig.

3A1 solid line) and 33µA (Fig. 3A2 solid line), respectively. After treating the cells by higher doses of MBZ (10.5 nM), the height of the CV and DPV spikes raised so sharp (Fig. 3B). The absolute DPV current reached to 150µA and 430µA, 4 and 24h after such treatment respectively (Fig. 3B2). Sharp electrochemical response of MCF-7 cells to MBZ incubation might be assigned to cells functional perturbations caused by drug induced MT depolymerization.

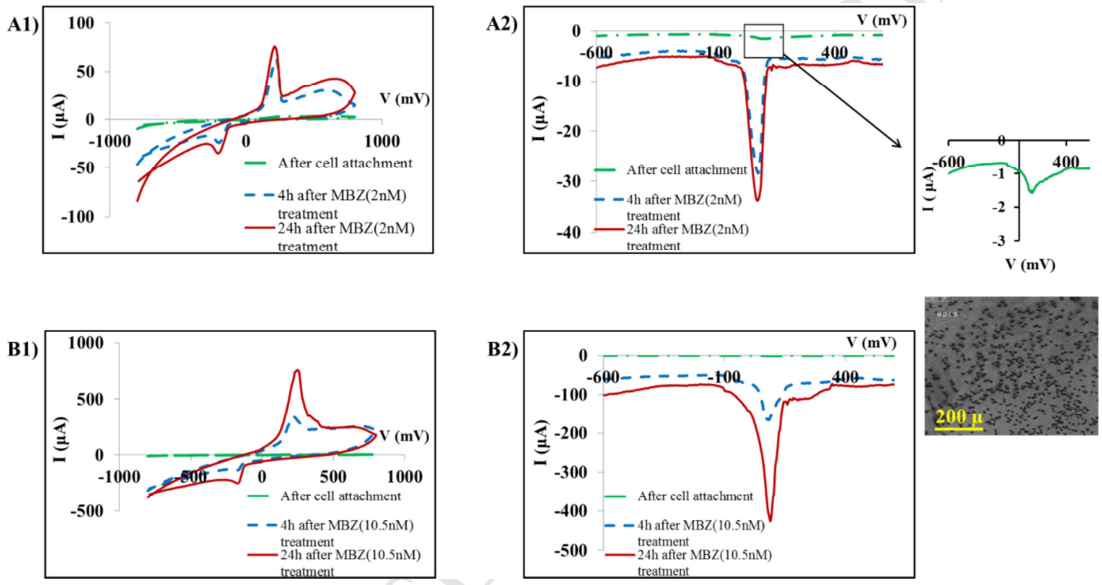

Fig. 3. A1) CV and A2) DPV spectra of SiNG WEs covered by MCF-7 cells and incubated by 2nM of MBZ in various time lapses after drug treatment. Time evolution led to increased spikes of the sensor. Similar experiment were done for individual sample treated with 10.5 nM of MBZ and results of panels (B1) and (B2) were obtained, respectively. The presence of cancer cells on nanograss electrodes was shown in FESEM image of panel A2. Dotted dashed, dotted and solid lines in each plot refer to cell attached (without drugs incubation), 4h and 24h after drug incubation, respectively.

Similarly, the sensor exhibited changed electrochemical spikes after incubating the cells with PTX drugs in various doses (Fig. 4). Treatment of attached MCF-7 cells with low doses of PTX (0.1 nM) for 4 hours, increased the anodic spike from 0.5 µA (Fig. 4A1 dotted dashed line) to 50µA (Fig. 4A1 dashed line). Also, DPV peak current of SiNGWEs reached to -12µA by such incubation. Increasing the PTX concentration to 1nM expressed the anodic response of the cells covered sensor to more than 100µA in just 4h (Fig. 4B1). Similar increment was observed in DPV current peaks (Fig. 4B2). Enhanced electrochemical responses of PTX treated sample were observed from 4hr to 24hr after drug incubation (Fig.4A1). This was similar to that of recorded for MBZ treated sample (Fig. 3A1).

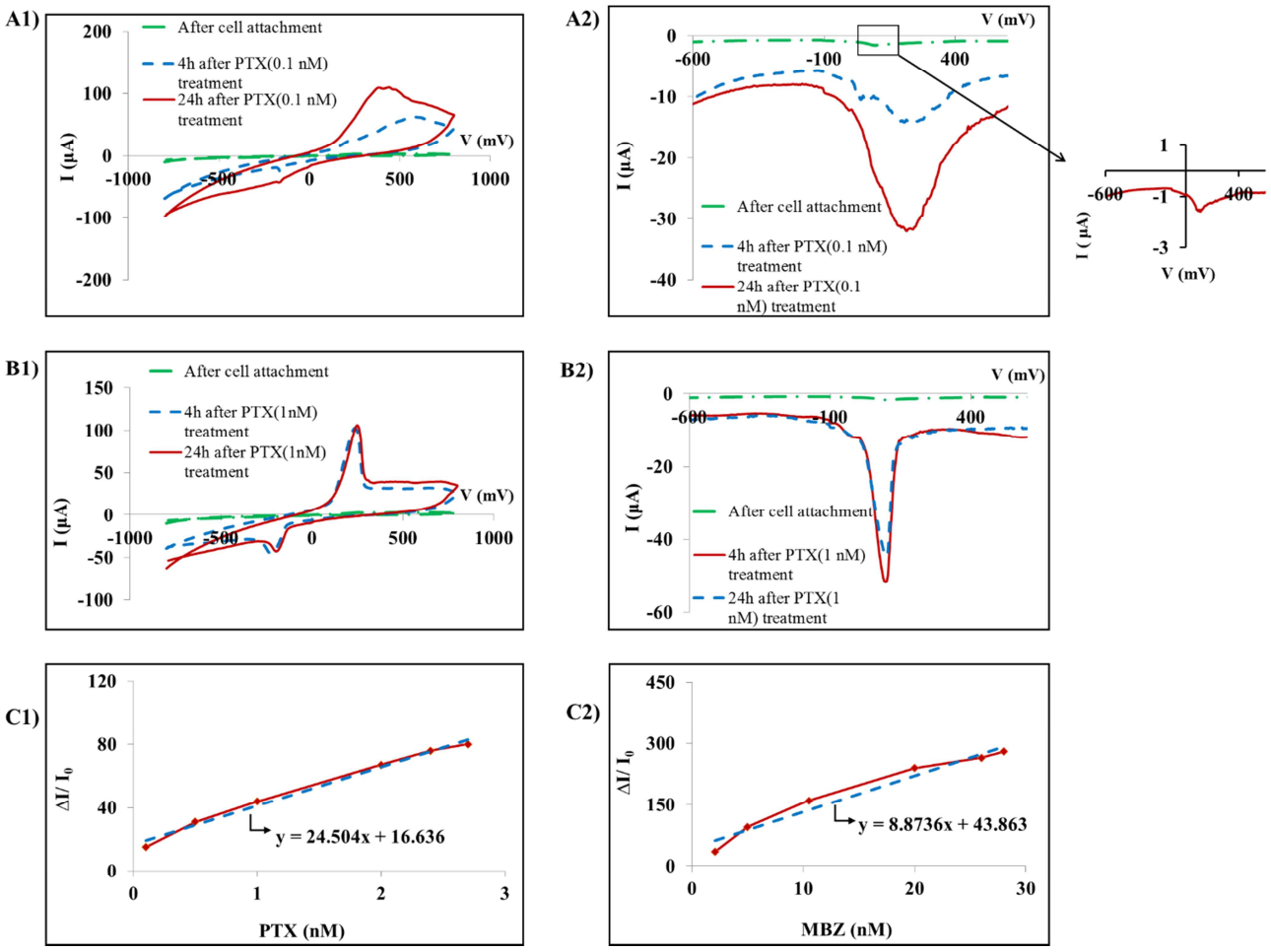

Fig. 4. CV and DPV spectra of SiNG electrochemical biosensor in various time lapses after interaction with 0.1 nM (A1 and A2) and 1nM (B1 and B2) of PTX. Drug treatment resulted in increasing electrochemical spikes but the intensity and strength of the spikes were different from MBZ treated samples. E) Detection limit profiles of the SiNG WEs in sensing the effect of MBZ and PTX are plotted in C1 and C2 panels, respectively. The detecting resolution followed the formulated regime is presented in each panel.

Similar charge mobility among the array of nanograsses, the excellent capability for exchange of charges at the tips [16], the great mobility of electrons in silicon crystalline structure [17] and/or considerable interactive surface between the grass and the cells might all be effective in the well sensitivity of SiNGWEs to electrochemical events induced in drug treated cancer cells.

To clarify the better charge exchange performance of SiNGWE in comparison with smooth silicon surface, we experimented chargeability of both surfaces by cyclic charge-discharge (CCD) technique. CCD is the standard approach used to test the performance and cyclic-life of a semiconductor electrode based on measuring the amount and rate of its chargeability in known interval of times [18]. A repetitive loop of charging and discharging is called a cycle. In this experiment, the charge and discharge were conducted at constant current (using Kimia Stat 123 Co.) until a set voltage was reached. The charge (capacity) of each cycle was measured and compared with the discharge of the surface determined by monitoring the voltage reduction in subsequent cycle. Fig. 5 shows CCD data recorded on SiNG (Fig. 5A1) and silicon (Fig. 5B1) surfaces, respectively. 10 cycles were recorded for SiNG in 40sec as indicated by voltage plotted versus time. The cycle numbers of silicon in the same time were less than 3 (Fig. 3B). Also,

much better charge exchange performance of SiNG would be observable by comparing its charge (Q) diagram (Fig. 3B1) with silicon (Fig. 3B2)."

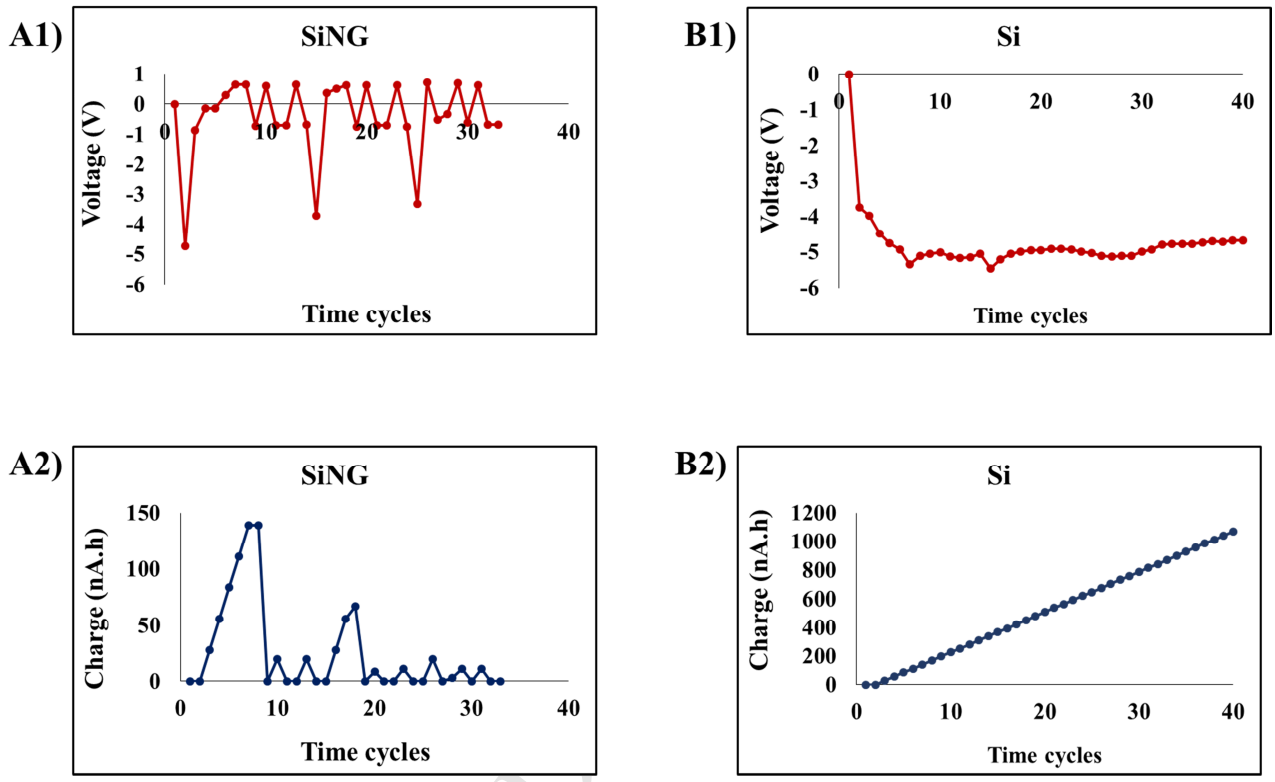

Fig. 5. Results of Cyclic voltammetry Charge-Discharge (CCD) technique to clarify the charge exchange performance of A1) SiNG electrodes in comparison with B1) bare Si electrodes. 10 cycles were achieved for SiNG in 40sec which indicats its well charge exchange rate (A2). Less than 3 incomplete cycles recorded for Si reveal its weak charge exchange performance (B2).

Detection limit

The detection limit profiles of the SiNGWEs in assaying the resistance of MCF-7 cells to MBZ (Fig. 4C1) and PTX (Fig. 4C2) drugs were presented by plotting the $\Delta I/I_0$ vs. concentration of the drugs. $\Delta I/I_0$ is defined as the ratio of the peak current obtained after subtraction of the background current in DPV from the typical current resolution of the WE treated by various concentrations of MBZ and PTX (here, 1 nA). Results indicate that the detectivity of SiNGWEs follows linear regime in the selected range of concentrations for both types of drugs. By linear

fitting the experimental data, the equations presented in Fig. 4C1 and C2 were obtained for current response as a function of drug concentration. The doses which induce less than 15 nA changes in the DPV response of the MCF-7 covered sensor wouldn't be detected by the sensor.

3.4. Electrochemical Mechanism of drug Effect

Many hypotheses were reported about the action mechanism of anti-tubulin drugs on cancer cells, all of which indicated on activation of one or more cellular signaling pathways such as Bcl phosphorylation, caspase3, 8 and9 [19], p53 [20] and release of cytochrome C from mitochondrial membrane to cytoplasm [14, 21]. We found that all of biochemical pathways have an electrochemical translation. As a result, MBZ treatment would change the anodic/cathodic response peaks of the biosensor covered by cancer cells. We know that caspase inhibition was frequently found to prolong the duration of mitosis [22]. Some investigations reported consecutive activation of more than one pathway as exposure to MBZ resulting in cytochrome C accumulation, activation of caspase-9 and caspase-8, and cleavage of PARP and procaspase-3 [21].

Some reports revealed that the fastest MBZ signaling goes through the mitochondrial Pathway. Accumulated cytochrome C in cytosolic region of MBZ treated cells, increased in a dose-dependent manner. After 12 hours from this accumulation, activation of caspase-9 and caspase-8 and cleavage of the caspase substrate poly (ADP-ribose) polymerase and procaspase-3 were detectable [14].

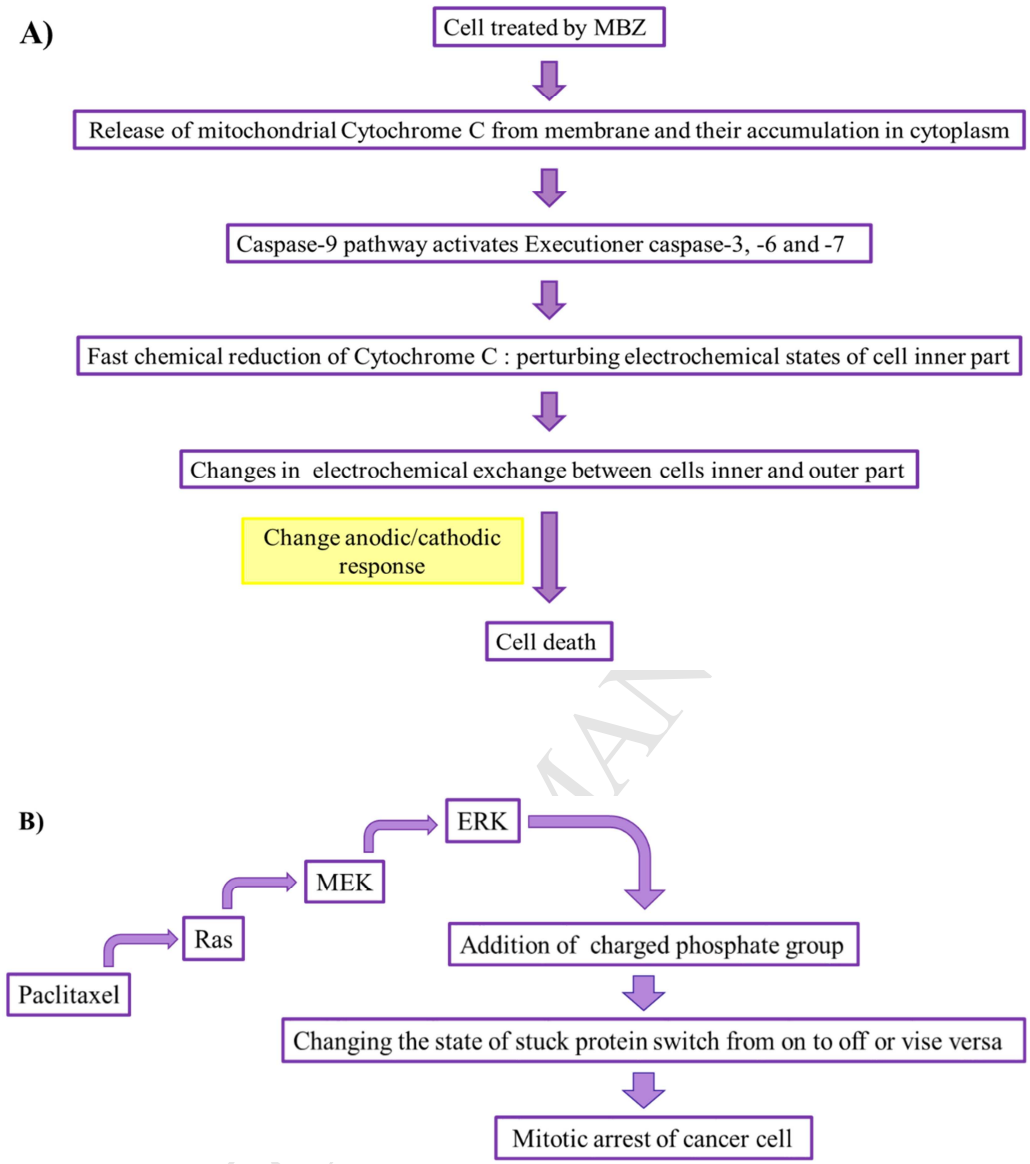

Fig. 6. A) Schematics from the electrochemical effect of MBZ on MCF-7 cells. Accumulation of cytochrome C from the mitochondrial membrane to the cytoplasm induced perturbations in the cell's ionic states. The schematic elaborated the reason of such changed electrochemical response of the sensor 4h after drug treatment. B). Schematic of paclitaxel-induced effects upon signal transduction pathways. Paclitaxel induced mitotic arrest by activation of caspase-7. Attachment of phosphate groups as charged molecules to the neighboring protein by ERK pathway (as the main agent of changing the state of the stuck switched protein in cancer transformed cells.) varied the ionic state of cells inner part which led to changed electrochemical response of the biosensor.

Cytochrome C is an active ionic agent which would rapidly be reduced in cytoplasm [23]. As MBZ incubation increased the accumulation of cytochrome C in cytosol, their fast chemical reduction would change the ionic state of the cells and subsequently electrochemical ion exchange would be occurred between cells and ionic media. Such exchange would alter the electrochemical response of the biosensor (Fig. 6).

As seen in Fig. 3, the DPV peaks of cancer cells incubated with low and high doses of MBZ indicates that increasing the dose of MBZ results in further releasing of cytochrome C and sharper changes in anodic response of the sensor. This suggests that electrochemical approach is in a well corroboration with the illustrious fact that depolymerization of MTs by MBZ alters membrane potential and disturbs the motional freedom of membrane proteins [24] which result in perturbing the function of Na^+ ion channels.

Also, an electrochemical event is existed behind the mitotic arrest activation in cancer cells after PTX treatment. Studies by a number of laboratories have also linked suppression of mitogen-activated protein kinase/extracellular signal-regulated kinase ($MEK^{1/2}$) pathway to enhanced PTX toxicity in vitro and in vivo. Chemical interaction between taxolarate and the $MEK^{1/2}$ inhibitor PD184352 in a sequence dependent fashion led to synergically mitotic arrest of MCF-7 cells [25]. Such interaction induces considerable changes in electrochemical state of cancer cells by activation of extracellular signal-related kinases ($ERK^{1/2}$) due to activation of caspase-7 [25] but not caspase-3 [26]. The mitotic induced pathway starts when a signaling molecule binds to the receptor on the cell surface and ends when the DNA in the nucleus expresses a protein and produces some change in the cell, such as cell division. The activated proteins in the ERK pathway add a phosphate groups to a neighboring protein, which acts as an "on" or "off" switch. Mutation in any of the mentioned proteins results in their sticking in “on” or “off” positions and

finally cancer transformation in the cell. PTX treatment (interaction of taxolarate with the pathway) could reverse such switch and induce mitotic arrest in cancer cells [27]. As the phosphate groups are charged molecules in the cells (phosphate group is the negatively-charged polar head which is hydrophilic), any variations in the state of the protein switches and probable addition of charged phosphate groups would strongly perturb the ionic equilibrium of the cell. In this regard, cell tends to exchange ions to maintain its ionic equilibrium and this would finally affect the anodic/cathodic response of the sensor covered by PTX treated cells.

3.5. Confocal and flowcytometry assays of drug treated cancer cells

Confocal imaging could indicate any disorders in tubulin assemblies of drug treated cells in comparison with non-treated ones (Fig.7). Mitotic suppressive pathways release cytochrome C in cytoplasm (in MBZ treated cells) and bind phosphate group to the proteins of cancer cells to switch them from their stuck state (in PTX treated cells), disturbing the microtubule associated proteins (Such as LC3 [28]) and inducing disorders in depolymerization/polymerization rate of MTs. Depolymerized tubules resulted in bright view of tagged nucleus in MBZ treated cells meanwhile presence of non-disturbed MTs in CTRL sample made the confocal view of the nucleus so blare (Fig. 7.A2,B2,C2) in which the trace of conformally distributed MTs prevented from observing the nucleus. Moreover, in PTX treated samples, increased aggregation in MT spindles are observable (Fig. 7C) which made the nucleus view non obvious in contrast to MBZ Treated sample (with abnormally reduced numbers of MT spindles). Similar to confocal images, FESEM micrographs taken from the MCF-7 cells (attached on SiNGWEs) 10hr after treatment with low doses of the mentioned drugs indicated changed morphology of treated cells vs. CTRL

sample. MBZ treated cell has been deformed and trace of the nucleus is observable as the result of MT depolymerization (Fig. 7B3). In contrast, CTRL cell maintained its conformal shape and hemogenic distribution (Fig. 7A3). Also, morphology of PTX treated cell exhibited dense composition of MTs as the result of polymerization (Fig. 7C3).

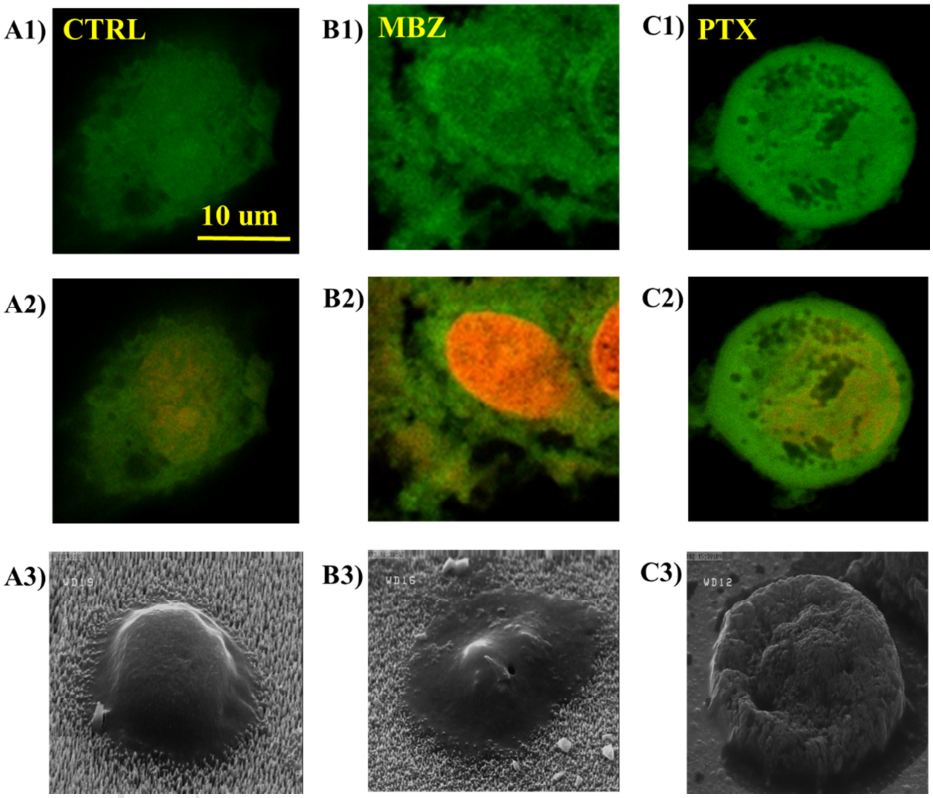

Fig. 7. Confocal microscopy images from the tubulin assemblies of **A1**) 2.1 nM MBZ **B1**) MCF-7 cells in CTRL state in comparison with and **C1**) 0.1 nM PTX treated samples in same times (4h after drug treatment). Extensive depolymerization and polymerization rate in MTs resulted in non-regular spindle formation in MBZ and PTX treated samples, respectively. Panels A2, B2 and C2 presents the combined confocal images from nucleus and MTs of MBZ, CTRL and PTX treated samples. It can be seen that the trace of nucleus is completely observable in MT depolymerized sample (MBZ treated cell) because tubulins which were in front of the nucleus have been degraded. Also FESEM images of the similar cells

presented in A2, B2 and C2 panels, respectively indicated the normal shape of CTRL sample (B3). The cytoskeletal shape of MBZ treated cell was degraded (A3) meanwhile for PTX treated sample it has been squeezed (C3).

In addition, cells vital state and cycle distribution were measured by flow cytometry analysis. Results are presented in Fig. 8, indicating that MBZ and PTX induced non similar effects on the cycles and states of the cells in comparison with control sample. As evident from Fig. 8, the subG_1 fraction, which is an indicator of apoptotic cells with hypodiploid DNA [29,30], increases dose dependently in MBZ treated samples with respect to CTRL sample (Apoptotic part in Fig. 8A vs. Figs. 8B1 and B2). This reveals that higher doses of MBZ induce apoptotic behavior in MCF-7 cells. However, such fraction didn't change in PTX treated samples neither in low nor high doses.

Also, proportion of G_0/G_1 fraction changed in MBZ incubated samples due to the dose of treatment. The peak of G_0/G_1 was 1500 in CTRL sample (Fig. 8A1) meanwhile it was reduced to 1000 and 800 in MBZ treated cells with the concentrations of 2.1 and 10.5 nM (Fig. 8B1 and B2). No noticeable changes was observed in G_0/G_1 fraction of PTX treated sample with low doses (0.1nM) meanwhile such fraction reduced to 1000 in high dose treated sample (1nM). Flow cytometry results completely corroborated the electrochemical responses of drug treated cells in which the variations in anodic spikes of MBZ treated sample were strongly sharper than that of treated by PTX (Fig. 3 vs. Fig. 4). So, a direct relation exists between flow cytometry result and the intensity of anodic spikes. Increased apoptotic and G_0/G_1 fractions directly correlated with increased anodic spikes in CV measurements. This reveals that electrochemical function of the cells presented a well correlation with cells cycle and vital state.

The result was confirmed by side scatter versus forward scatter (SSC-FSC) diagram as a strong sign of cells granularity [30] (Right panels in Fig. 8). Fine scatter plot in CTRL and PTX treated samples reveal their better granularity with respect to MBZ treated samples with wide scatter plots. Also, a quick glance to the SEM images of MBZ (High dose) treated samples, indicates their non-granule shape (Fig. 8D2) in comparison with CTRL sample (Fig. 8D1).

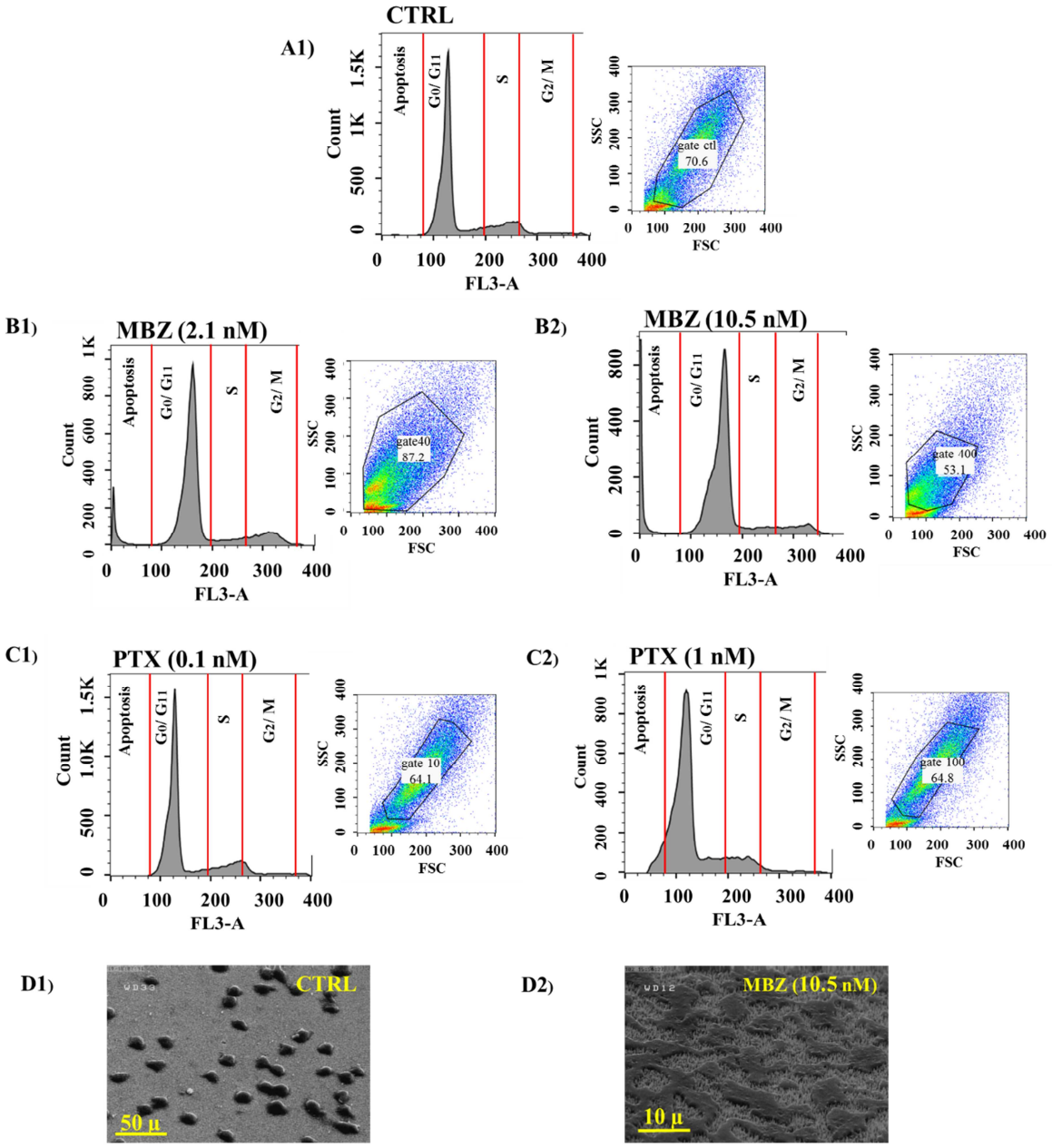
A1)
CTRL
Apoptosis
G0/ G11
S
G2/ M
Count
FL3-A
SSC
FSC
gate ctl
70.6
B1)
MBZ (2.1 nM)
gate40
87.2
B2)
MBZ (10.5 nM)
gate 400
53.1
C1)
PTX (0.1 nM)
gate 10
64.1
C2)
PTX (1 nM)
gate 100
64.8
D1)
CTRL
50 µ
D2)
MBZ (10.5 nM)
10 µ

Fig. 8. Flowcytometry analyses of MCF-7 cells in (A1) No drug, (B1) MBZ 2.1 nM, (B2) MBZ 10.5 nM, (C1) PTX 0.1nM and (C2) PTX 1 nM treated states. The cell's fractions in apoptotic, G0/G1, S and G2/M cycles are observable in all of panels. MBZ treatment reduced the vitality of the cells and PTX treatment perturb the cells cycle. R1 region (presented in the right of each panel) indicated the state of counted cells. Also SSC vs. FSC plots, presented in the right panel of each plot, revealed the non-granular shape of MBZ treated samples in comparison with others. Such non granularity was indicated in comparative FESEM images of CTRL (D1) and MBZ (10.5 nM) treated samples.

If we take comparative consideration between flow cytometry and electrochemical data of the samples, a great complied result could be observed. The apoptotic fraction count of MBZ (10nM) treated cells was 800 (Fig. 8B2) meanwhile such count was less than 40 for CTRL (Fig. 8a) and PTX treated (Fig. 8C2) cells. This reveals that the number of the cells entered into apoptotic cycle after over expression of the cytochrome C releasing pathways (activated in MBZ treated cells) were increased. The pathway induced ionic exchanges between cell and peripheral media. On the other hand, the cathodic spikes of MBZ treated cells reached to 350µA in just 4hr (Fig. 3B1) meanwhile such values were about 5 µA (green solid curves in Fig. 3B1 and 4B1) and 80µA (Fig. 3B1) in CTRL and PTX treated cells, respectively. Therefore, increment in apoptotic fraction would be related to the increased electrochemical spikes in depolymerizing drug treated samples with respect to that in CTRL and polymerizing drug treated samples.

In addition, as we stated before, PTX treatment just induced mitotic arrest by the electrochemically translatable pathway. If we compare the flow cytometry diagrams of PTX treated sample (Fig. 8B) with CTRL one (Fig. 8A), changed G_0/G_1 and S cycles (which involve in presenting the mitotic behavior of the cells) would be observable. The intensity of the G_0/G_1 cycle was reduced from 1.5k (Fig. 8A) to 0.8k (Fig. 8B2) after 4hr incubating the cells by PTX (1nM). Also, the ratio of $S/(G_0/G_1)$ cycles increased in PTX treated sample with respect to CTRL

ones. This indicates that the PTX treated cells were arrested in S cycle and didn't continue their mitosis to refill the G_0/G_1 fraction. Such perturbations observed in flow cytometry are in a well match with increased cathodic spikes of PTX treated sample (Fig. 3B2, green vs. blue). However, the cathodic spikes of PTX treated cells were at least 4 times lower than MBZ treated sample (Fig. 3B1 vs. Fig. 4B1). Thus, we can deduce that apoptotic induction would make stronger effects than mitotic arrestment on electrochemical response of the drug treated cells. Based on this discussion, flow cytometry exhibited a well matching with electrochemical response of drug treated cells.

4. Conclusion

In summary, silicon nanograss surface in the architecture of working electrode was applied to detect the effect of antitubulin drugs on cancer cells. Mebendazole and Paclitaxel as microtubule depolymerizing and polymerizing agents, affect the ionic function of MCF-7 cells by various signaling pathways. The changed electrochemical response of biological medium, induced from drug treatment of the cells, was detected by monitoring the cyclic voltammetry and Differential Pulse Voltammetry of nanograss based sensor. Drug treatment affected both anodic and cathodic spikes of the silicon nanograss working electrodes covered by MCF-7 cells. The changed responses were in a well match with biological pathways activated in the cells by drug treatment as discussed in the paper. Also, the flow cytometry corroborated the correlation between different electrochemical responses of the mebendazole and paclitaxel treated cells and the

distribution of the cells' cycles. The device detected the trace of mebendazole (2nM) and paclitaxel (0.1nM) by exhibiting 250 and 100 nA changes in electrochemical peaks of the sensors respectively. This would be a new bioelectronics approach in the field of cancer detection and therapeutics.

References

[1] M. Turner, M. Londei, M. Feldmann, Human T cells from autoimmune and normal individuals can produce tumor necrosis factor., Eur. J. Immunol. 17 (1987) 1807–1814. doi:10.1002/eji.1830171220.

[2] R. Gupta, N.K. Chaudhury, Entrapment of biomolecules in sol–gel matrix for applications in biosensors: Problems and future prospects, Biosens. Bioelectron. 22 (2007) 2387–2399. doi:10.1016/j.bios.2006.12.025.

[3] M. Hepel, C.-J. Zhong, eds., Functional Nanoparticles for Bioanalysis, Nanomedicine, and Bioelectronic Devices, Volume 1, American Chemical Society, Washington, D.C., 2012. doi:10.1021/bk-2012-1112.

[4] C. Zhu, G. Yang, H. Li, D. Du, Y. Lin, Electrochemical Sensors and Biosensors Based on Nanomaterials and Nanostructures, Anal. Chem., 87 (2014) 230-49. doi: 10.1021/ac5039863 .

[5] C.B. Jacobs, M.J. Peairs, B.J. Venton, Review: Carbon nanotube based electrochemical sensors for biomolecules, Anal. Chim. Acta. 662 (2010) 105–127. doi:10.1016/j.aca.2010.01.009.

[6] F. Li, J. Peng, J. Wang, H. Tang, L. Tan, Q. Xie, S. Yao, Carbon nanotube-based label-free electrochemical biosensor for sensitive detection of miRNA-24, Biosens. Bioelectron. 54 (2014) 158–164. doi:10.1016/j.bios.2013.10.061.

[7] J. Bauer, F. Fleischer, O. Breitenstein, L. Schubert, P. Werner, U. Gösele, M. Zacharias, Electrical properties of nominally undoped silicon nanowires grown by molecular-beam epitaxy, Appl. Phys. Lett. 90 (2007) 012105. doi:10.1063/1.2428402.

[8] Y. Qu, L. Liao, Y. Li, H. Zhang, Y. Huang, X. Duan, Electrically Conductive and Optically Active Porous Silicon Nanowires, Nano. Lett. 9 (2009) 4539-43. doi: 10.1021/nl903030h .

[9] K.-I. Chen, B.-R. Li, Y.-T. Chen, Silicon nanowire field-effect transistor-based biosensors for biomedical diagnosis and cellular recording investigation, Nano Today. 6 (2011) 131–154. doi:10.1016/j.nantod.2011.02.001.

[10] H. Abiri, M. Abdolahad, M. Gharooni, S. A. Hosseini, M. Janmaleki, S. Azimi, M. Hosseini, S. Mohajerzadeh, Monitoring the Spreading Stage of Lung Cells by Silicon Nanowire Electrical Cell Impedance Sensor for Cancer Detection Purposes, Biosens. Bioelectron. 68 (2015) 577-585. doi:10.1016/j.bios.2015.01.057 .

[11] Q. Qing, Z. Jiang, L. Xu, R. Gao, L. Mai, C.M. Lieber, Free-standing kinked nanowire transistor probes for targeted intracellular recording in three dimensions, Nat. Nanotechnol. 9 (2013) 142–147. doi:10.1038/nnano.2013.273.

[12] M. Mehran, Z. Sanaee, M. Abdolahad, S. Mohajerzadeh, Controllable silicon nano-grass formation using a hydrogenation assisted deep reactive ion etching, Mater. Sci. Semicond. Process. 14 (2011) 199–206. doi:10.1016/j.mssp.2011.02.014.

[13] M. Abdolahad, H. Taghinejad, a. Saeidi, M. Taghinejad, M. Janmaleki, S. Mohajerzadeh, Cell membrane electrical charge investigations by silicon nanowires incorporated field effect transistor (SiNWFET) suitable in cancer research, RSC Adv. 4 (2014) 7425. doi:10.1039/c3ra46272b.

[14] T. Mukhopadhyay, J. Sasaki, R. Ramesh, J.A. Roth, Mebendazole elicits a potent antitumor effect on human cancer cell lines both in vitro and in vivo., Clin. Cancer Res. 8 (2002) 2963–9. doi:10.1016/s0955-0674(96)80044-5.

[15] M. Abdolahad, H. Shashaani, M. Janmaleki, S. Mohajerzadeh, Silicon nanograss based impedance biosensor for label free detection of rare metastatic cells among primary cancerous colon cells, suitable for more accurate cancer staging., Biosens. Bioelectron. 59 (2014) 151–9. doi:10.1016/j.bios.2014.02.079.

[16] P.N. Rao, E.A. Schiff, L. Tsybeskov, P. Fauchet, Photocarrier drift-mobility measurements and electron localization in nanoporous silicon, Chem. Phys. 284 (2002) 129-138. doi: 10.1016/S0301-0104(02)00544-X .

[17] F. Schindler, M. C. Schubert, A. Kimmerle, J. Broisch, S. Rein, W. Kwapil, W. Warta, Modeling majority carrier mobility in compensated crystalline silicon for solar cells, Solar Energy Materials and Solar Cells. 106 (2012) 31-36. doi:10.1016/j.solmat.2012.06.018 .

[18] S. Gupta, M. vanMeveren, J. Jasinski, Investigating Electrochemical Properties and Interfacial Processes of Manganese Oxides/Graphene Hybrids as High-Performance Supercapacitor Electrodes, Int. J. Electrochem. Sci. 10 (2015) 10272-10291.

[19] T. Ona, J. Shibata, Advanced dynamic monitoring of cellular status using label-free and non-invasive cell-based sensing technology for the prediction of anticancer drug efficacy, Anal. Bioanal. Chem. 398 (2010) 2505–2533. doi:10.1007/s00216-010-4223-5.

[20] Z. Wang, Y. Sun, Targeting p53 for Novel Anticancer Therapy., Transl. Oncol. 3 (2010) 1–12.

[21] P. Pantziarka, G. Bouche, L. Meheus, V. Sukhatme, V.P. Sukhatme, Repurposing Drugs in Oncology (ReDO)-mebendazole as an anti-cancer agent., Ecancermedicalscience. 8 (2014) 443. doi:10.3332/ecancer.2014.443.

[22] K.E. Gascoigne, S.S. Taylor, How do anti-mitotic drugs kill cancer cells?, J. Cell Sci. 122 (2009) 2579–85. doi:10.1242/jcs.039719.

[23] M.O. Ripple, M. Abajian, R. Springett, Cytochrome c is rapidly reduced in the cytosol after mitochondrial outer membrane permeabilization, Apoptosis. 15 (2010) 563–573. doi:10.1007/s10495-010-0455-2.

[24] K.E. Herold, A. Rasooly, Biosensors and molecular technologies for cancer diagnostics, CRC Press, 2012.

[25] J. D. Orth, A. Loewer, G. Lahav, T. J. Mitchison, Prolonged mitotic arrest triggers partial activation of apoptosis, resulting in DNA damage and p53 induction, Mol. Biol. Cell. 23 (2012) 567-576. doi: 10.1091/mbc.E11-09-0781

[26] R. Ofir, R. Seidman, T. Rabinski, M. Krup, V. Yavelsky, Y. Weinstein, M. Wolfson, Taxol-induced apoptosis in human SKOV3 ovarian and MCF7 breast carcinoma cells is caspase-3 and caspase-9 independent, Cell Death and Diff. 9 (2002) 636-642. doi: 10.1038/sj/cdd/4401012

[27] A. Yacoub, D. Gilfor, W. Hawkins, M.A. Park, D. Hanna, M.P. Hagan, D.T. Curiel, P.B. Fisher, S. Grant, P. Dent, MEK1/2 inhibition promotes Taxotere lethality in mammary tumors in vivo., Cancer Biol. Ther. 5 (2006) 1332–9. doi:10.4161/cbt.5.10.3215 .

[28] I. Tanida, T. Ueno, E. Kominami, LC3 and Autophagy., Methods Mol. Biol. 445 (2008) 77–88. doi:10.1007/978-1-59745-157-4_4.

[29] Z. Pan, A. Avila, L. Gollahon, Paclitaxel induces apoptosis in breast cancer cells through different calcium--regulating mechanisms depending on external calcium conditions., Int. J. Mol. Sci. 15 (2014) 2672–94. doi:10.3390/ijms15022672.

[30] A. Aszalos, S. Damjanovich, M.M. Gottesman, Depolymerization of microtubules alters membrane potential and affects the motional freedom of membrane proteins, Biochemistry. 25 (1986) 5804–5809. doi:10.1021/bi00367a069.

Highlights

Electrochemical effect of MBZ and PTX (anti tubulin drugs) on breast cancer cells was detected.

Detection was carried by silicon nanograss electrodes(SiNGEs).

Signaling pathways activated in the cells by drug treatment, change the anodic/cathodic response of cells covered SiNGEs.

Cytochrome C and $ERK^{1/2}$ play the crucial role in changed electrochemical responses of MBZ and PTX treated cells respectively.